Transient activation of the HOG MAPK pathway regulates bimodal gene expression

Pelet, S ; Rudolf, F ; Nadal-Ribelles, M ; de Nadal, E ; Posas, F ; Peter, M

Abstract: Mitogen-activated protein kinase (MAPK) cascades are conserved signalling modules that control many cellular processes by integrating intra- and extracellular cues. The p38/Hog1 MAPK is transiently activated in response to osmotic stress, leading to rapid translocation into the nucleus and induction of a specific transcriptional program. When investigating the dynamic interplay between Hog1 activation and Hog1-driven gene expression, we found that Hog1 activation increases linearly with stimulus, whereas the transcriptional output is bimodal. Modelling predictions, corroborated by single cell experiments, established that a slow stochastic transition from a repressed to an activated transcriptional state in conjunction with transient Hog1 activation generates this behaviour. Together, these findings provide a molecular mechanism by which a cell can impose a transcriptional threshold in response to a linear signalling behaviour.

DOI: https://doi.org/10.1126/science.1198851

Transient activation of the HOG MAPK pathway regulates bimodal gene expression

Serge Pelet[1,*], Fabian Rudolf[1,2], Mariona Nadal-Ribelles[3], Eulàlia de Nadal[3], Francesc Posas[3], and Matthias Peter[1,*]

[1] *ETH-Zurich, Department of Biology, Institute of Biochemistry, Schafmattstr. 18, CH-8093 Zurich, Switzerland*

[2] *present address: D-BSSE, ETH-Zurich, Mattenstr. 26, CH-4058 Basel, Switzerland*

[3] *Cell Signaling Unit, Departament de Ciències Experimentals i de la Salut, Universitat Pompeu Fabra, E-08003 Barcelona, Spain.*

[*] to whom correspondence should be addressed:

SP (serge.pelet@bc.biol.ethz.ch) or MP (matthias.peter@bc.biol.ethz.ch)

The authors declare that they have no competing financial interests.

Mitogen-activated protein kinase (MAPK) cascades are conserved signalling modules that control many cellular processes by integrating intra- and extra-cellular cues. The p38/Hog1 MAPK is transiently activated in response to osmotic stress, leading to rapid translocation into the nucleus and induction of a specific transcriptional program. When investigating the dynamic interplay between Hog1 activation and Hog1-driven gene expression, we found that Hog1 activation increases linearly with stimulus, whereas the transcriptional output is bimodal. Modelling predictions, corroborated by single cell experiments, established that a slow stochastic transition from a repressed to an activated transcriptional state in

conjunction with transient Hog1 activation generates this behaviour. Together, these findings provide a molecular mechanism by which a cell can impose a transcriptional threshold in response to a linear signalling behaviour.

Mitogen-activated protein kinase (MAPK) cascades orchestrate many cellular processes including cell growth, division and differentiation (*1*). In *S. cerevisiae*, the high osmolarity glycerol (HOG) pathway is needed to re-establish the balance between internal and external pressures upon osmotic shock (*2*). Osmo-sensors at the cell membrane activate either the MAPK kinase kinases (MAPKKK) Ste11 or Ssk2,22, which converge on the MAPKK Pbs2. In turn, Pbs2 doubly phosphorylates the MAPK Hog1, leading to rapid translocation into the nucleus to launch a transcriptional program. Although increased transcription is essential to survive very high osmotic stress (0.8M NaCl), it is not required for milder stress conditions (0.4 M NaCl) (*3*), under which Hog1 kinase activity alone is sufficient to drive cellular adaptation. In contrast, in the yeast mating MAPK pathway, transcription and new protein expression are required for cell cycle arrest and mating (*4*).

Transcriptional activation of mating genes occurs with linear kinetics and high fidelity (*5, 6*), and the observed cell-to-cell variation in protein expression is governed by the ability of cells to express proteins (expression capacity) (*5*). While the mating pathway can be compared to a cell-fate decision system with sustained MAPK activity, the HOG pathway is an adaptation response, which is only transiently induced like other stress-activated pathways (*7*). We therefore investigated whether this transient response would trigger different expression behaviour.

To quantitatively measure the transcriptional output induced by osmotic stress, we engineered a reporter system based on a quadruple Venus (qV) fluorescent protein expressed under the control of specific osmo-stress-inducible promoters dependant on the three main transcription factors orchestrating the transcriptional response to osmotic

stress (Hot1 and Sko1: p*STL1*, Msn2,4: p*ALD3* or Msn2,4 and Hot1: p*HSP12*) (*8*). Flow cytometry revealed a Pbs2-dependent 20-fold increase in p*STL1*-qV reporter expression when 0.4M NaCl was added to the growth medium (Fig. 1 A and B). No expression was detected at low salt concentrations (below 0.05M), while above 0.15M, all cells expressed the reporter and the amount of fluorescence increased linearly with stress. However, at intermediate concentrations, we observed histograms with two distinct sub-populations representing non-expressing cells with basal autofluorescence levels and expressing cells with higher intensities. These distributions are termed bimodal. The p*ALD3*-qV and p*HSP12*-qV reporters displayed a similar bimodal expression behaviour (Fig. 1B and Fig. S1A). Induction of the mating pathway for 45 minutes with α-factor also generated a bimodal expression output of the Ste12-specific reporter p*FIG1*-qV. However, signalling in the mating pathway is prevented from "Start" through S phase (*9*), and expression output became unimodal after relieving this cell-cycle dependent restriction (Fig. 1B and Fig. S1B).

To investigate the source of the HOG pathway bimodal expression behaviour, we integrated two reporters driving the expression of a quadruple cyan fluorescent protein (qCFP) and a qV construct in the same cell. Correlation of the cyan and yellow intensities measures the contribution of cell-to-cell (extrinsic) and intra-cellular (intrinsic) variability to the overall expression noise (*5, 10*). The two p*FIG1*-reporters induced by α-factor demonstrated that the mating pathway is governed by extrinsic noise. In contrast, we observed a lack of correlation between the two p*STL1*-reporters (Fig. 1C-E and Fig. S2), demonstrating that the bimodal expression behaviour of the HOG-pathway is independent of cell-to-cell variability caused by extrinsic factors such as expression capacity or cell cycle stage.

To assess the observed bimodality and Hog1-signalling simultaneously, we combined a Hog1-relocation assay (*11, 12*) with the p*STL1*-qV expression reporter (Fig.

2A). Because nuclear accumulation of Hog1 is linked to its kinase activity (*13*), this assay allows correlating in each cell the signalling and expression outputs (Fig. 2B and C). When cells were stressed with increasing salt concentrations, Hog1 nuclear accumulation gradually augmented both in magnitude and retention time. At the single cell level, a clear discrepancy was apparent between the linear increase in signalling output versus the bimodal behaviour observed in the expression output (Fig. 2D-F and Fig. S3). We conclude that Hog1 activation as measured by its nuclear translocation is not sufficient to induce a defined transcriptional output, indicating that unknown intracellular factor(s) set a threshold for gene expression.

Hog1 has been implicated at various steps in the complex mechanisms leading to gene transcription (*14, 15*). First, Hog1 associates with transcription factors that bind at specific promoters (*16*). The MAPK then recruits RNA polymerase PolII as well as chromatin remodelling complexes such as SAGA (Spt-Ada-Gcn5 Acetyltransferase) and RSC (Chromatin Structure Remodelling), which evict nucleosomes (*17-19*). During active transcription, the INO80 complex and histone chaperones are involved in redeposition of histones, and therefore help silencing these genes once stress has been overcome (*20*).

To test if bimodality is reflected in chromatin remodelling, we used chromatin-immunoprecipitation (ChIP) to monitor the occupancy of histone H3 on the *STL1*, *HSP12* and *ALD3* promoters. Histone eviction occurred in a Hog1-dependent manner (Fig. S4A and (*18*)) and it was complete from 0.15M (*STL1*, *ALD3*) or 0.2M NaCl (*HSP12*) (Fig. 3A). The partial eviction observed at low stress levels suggests that only a fraction of the population was able to remodel chromatin to allow for efficient transcription. In contrast to other transcription regulators such as Asf1, Cyc8 or Htz1, the bimodal behaviour of the p*STL1*-qV stress-reporter was already present in the absence of stress in cells deleted for the INO80 subunit Arp8 (Fig. 3B, Fig S5A and B and Table S1). Conversely, bimodality

was significantly increased in cells with impaired SAGA or RSC function (Fig. 3B and Fig. S6), indicating that chromatin remodelling activity affects the threshold of gene expression. We verified that eviction of histone H3 is incomplete in *gcn5*Δ cells (Fig. 3C and Fig. S4B), reinforcing the notion that the partial histone eviction observed at the population level is linked to the bimodal expression measured in single cells.

Deletion of either of the two transcription factors Sko1 and Hot1 strongly reduced p*STL1*-qV expression and led to a bimodal expression pattern at high stress levels (Fig. S5C). This behaviour could be partially rescued by the additional deletion of *ARP8*. Moreover, cells grown at low glucose concentration (0.05%) where glucose repression is alleviated display a bimodal transition around 0.05M NaCl (Fig. S7A-C). The bimodal transition shifts to higher stress levels as glucose repression increases with the amount of glucose in the medium. Taken together, these results suggest that the bimodality depends on a number of dynamic processes cooperating at stress-induced promoters to regulate the activation of the transcription.

To better understand the dynamics of gene activation, we designed a simple stochastic model of Hog1-induced transcription (Fig. S8 and SOM Text), which identified the formation of an active gene complex (i.e. a gene with open chromatin which can be efficiently transcribed) as the crucial step governing the bimodal expression pattern. As predicted by the model, a transient activation of the HOG pathway for specific lengths of time with high stresses revealed a bimodal distribution of p*STL1*-qV reporter expression at early time points (Fig. 4A and C). Microscopy analysis confirmed that these conditions result in short-lived nuclear relocation of Hog1 in all cells and a bimodal expression response of the population (Fig. 4D and E). Conversely, sustained activation of Hog1 with low stresses using a ramping protocol resulted in a transition from non-expressing to fully expressing cells going through a bimodal stage (Fig. 4B-E).

We conclude that both the retention time and concentration of Hog1 in the nucleus are critical parameters that control bimodality of the transcription of stress-activated genes.

Stress-genes have to fulfil two contradictory requirements, which may explain their large noise in expression (*21, 22*). First, under normal growth conditions these genes are silenced, although basal pathway activity can be present (*23, 24*). Second, upon stress, these genes have to be expressed at a high rate to contribute to the adaptation of the cell during the short period of activity of the pathway. Importantly, bimodal gene expression may be a general feature of stress-induced genes, as oxidative or heat stresses also generated a bimodal expression pattern (Fig. S9).

If the approx. 300 genes induced by osmotic stress (*8*) were expressed in a stochastic fashion, a unique set of 150 genes would be present in each cell. Fluorescence reporter expression can therefore not be linked to increased resistance to osmotic stress and we failed to detect a pattern in reporter expression in cells subjected to two subsequent mild osmotic stresses (Fig. S10). However, this broad diversity in expression pattern will result in a large variability in protein content of the cells, which could be advantageous to survive in changing environments (*25*). Thus, noise in stress gene expression may confer an evolutionary advantage to a population by increasing fitness to face a large range of stress events.

References

1. R. E. Chen, J. Thorner, Biochim Biophys Acta **1773**, 1311 (2007).
2. S. Hohmann, M. Krantz, B. Nordlander, Meth Enzymol **428**, 29 (2007).
3. P. J. Westfall, J. C. Patterson, R. E. Chen, J. Thorner, Proc Natl Acad Sci USA **105**, 12212 (2008).
4. L. J. Oehlen, J. D. McKinney, F. R. Cross, Molecular and Cellular Biology **16**, 2830 (1996).
5. A. Colman-Lerner et al., Nature **437**, 699 (2005).
6. R. C. Yu et al., Nature **456**, 755 (2008).
7. A. P. Gasch et al., Mol Biol Cell **11**, 4241 (2000).
8. A. P. Capaldi et al., Nat Genet **40**, 1300 (2008).
9. S. C. Strickfaden et al., Cell **128**, 519 (2007).
10. M. B. Elowitz, A. J. Levine, E. D. Siggia, P. S. Swain, Science **297**, 1183 (2002).
11. D. Muzzey, C. A. Gómez-Uribe, J. T. Mettetal, A. van Oudenaarden, Cell **138**, 160 (2009).
12. P. Hersen, M. N. McClean, L. Mahadevan, S. Ramanathan, Proc Natl Acad Sci USA **105**, 7165 (2008).
13. P. Ferrigno, F. Posas, D. Koepp, H. Saito, P. A. Silver, EMBO J **17**, 5606 (1998).
14. E. de Nadal, F. Posas, EMBO J **29**, 4 (2010).
15. V. M. Weake, J. L. Workman, Nature Reviews Genetics **11**, 426 (2010).
16. E. Nadal, L. Casadome, F. Posas, Molecular and Cellular Biology **23**, 229 (2003).
17. P. M. Alepuz, E. de Nadal, M. Zapater, G. Ammerer, F. Posas, EMBO J **22**, 2433 (2003).
18. G. Mas et al., EMBO J **28**, 326 (2009).
19. M. Zapater, M. Sohrmann, M. Peter, F. Posas, E. de Nadal, Molecular and Cellular Biology **27**, 3900 (2007).
20. E. Klopf et al., Molecular and Cellular Biology **29**, 4994 (2009).
21. A. Bar-Even et al., Nat Genet **38**, 636 (2006).
22. J. R. S. Newman et al., Nature **441**, 840 (2006).

23. J. Macia et al., Science signaling **2**, ra13 (2009).
24. A. Loewer, E. Batchelor, G. Gaglia, G. Lahav, Cell **142**, 89 (2010).
25. L. López-Maury, S. Marguerat, J. Bähler, Nat Rev Genet **9**, 583 (2008).
26. We thank R. Dechant, C. Schüller, G. Ammerer, A Colman-Lerner and A. Smith for strains, plasmids and helpful discussions, S.-S. Lee and H. Koeppl for help with flow chamber experiments and model design, respectively. We are grateful to C. Rupp and D. Condé for technical assistance. This work was supported by QUASI, UNICELLSYS, the SystemsX.ch organization and the Competence Centre "Systems Physiology and Metabolic Disease" (CC-SPMD). M.N. is supported by ISCIII, and F.P is recipient of an ICREA Acadèmia (Generalitat de Catalunya) award. Work in the Posas and de Nadal laboratories is funded by the Fundación Marcelino Botín (FMB), and the Ministerio de Ciéncia y Innovación (BFU2008-00530 to E.N. and BIO2009-07762 to F.P.). The Peter laboratory is supported by the Swiss National Science Foundation and ETHZ.

Supporting Online Material

www.sciencemag.org

Materials and Methods

SOM Text

Figs. S1 to S11

Tables S1 to S5

References

Figure Legends

Fig. 1: Bimodal expression of fluorescent reporters upon osmotic stress.

(**A**) Dose response of the quadruple-Venus (qV) fluorescence reporter driven by the *STL1* promoter (p*STL1*) measured by flow cytometry. (**B**) Dose responses of wild-type or *pbs2Δ* cells harbouring the indicated osmo-stress inducible reporters driven by the *STL1*-, *ALD3*-, *HSP12*-promoters, or α-factor inducible reporter p*FIG1*-qV in a *cdc28-as* background with 1-NM-PP1 inhibitor (10μM) or DMSO. The mean of the log-normal distribution fitted to the flow cytometry histograms is plotted. The best fit between single or double log-normal distributions was selected for each curve. The open and closed circles represent, respectively, the population of non-reacting and reacting cells. Circle size is proportional to the population under each distribution. (**C** and **D**) Intrinsic and extrinsic noise revealed by microscopy in a strain that contains both CFP and YFP expression reporters driven by the p*STL1*-promoter stressed with 0.1M (red) or no (black) NaCl (C), or in *cdc28-as* cells inhibited by 1-NM-PP1 with expression reporters driven by the p*FIG1*-promoter treated with 0.03μM (red) or no (black) α-factor (D). (**E**) Percentage of intrinsic (grey) and extrinsic (white) noise over total noise quantified for osmotic stress or α-factor treatment in cells bearing two p*STL1*- or p*FIG1*-expression reporters, respectively.

Fig. 2: Comparison between Hog1 nuclear relocation and p*STL1*-qV reporter expression in single cells.

(**A**) Wild-type cells expressing the nuclear marker Hta2-CFP, Hog1-mCherry and the p*STL1*-qV expression reporter imaged before or after addition of 0.4M NaCl. (**B** and **C**) Quantification of single cell traces: the integral below the nuclear accumulation curve is used as a measure of the signalling output (B). The difference between final and initial

average intensity allows quantification of the expression output (C). (**D**) The signalling and expression outputs were quantified in single cells exposed to 0.1M (red) or no (black) NaCl. (**E** and **F**) Traces of three single cells marked in panel D displaying almost identical Hog1 relocation dynamics (E) but different expression outcomes (F).

Fig. 3: Influence of chromatin remodelling on reporter expression.

(**A**) Dynamics of histone H3 eviction at the *STL1*-, *ALD3*- and *HSP12*-promoters was measured by quantitative ChIP experiments after addition of the indicated NaCl concentration. Histone H3-binding was normalized to a *TEL2* sequence control. The error bars correspond to the standard deviation of three independent measurements. (**B**) Mean of the log-normal fit of flow cytometry histograms of p*STL1*-qVenus expression quantified in wild-type (wt), *arp8*Δ, *gcn5*Δ cells after addition of NaCl. (**C**) Histone H3 occupancy in wild-type and *gcn5*Δ cells was quantified as in (A) 5 min after osmotic stress.

Fig. 4: Duration and intensity of Hog1 nuclear accumulation controls bimodality.

(**A** - **C**) Flow cytometric measurement of p*STL1*-qV expression and mean of log-normal fits of the histograms (C) upon transient or sustained activation using a pulse of 0.2M NaCl (A) or a ramp from 0.05M to 0.4M NaCl (B). (**D**) Modulation of the Hog1 activation pattern in flow chambers studied by microscopy. Mean Hog1 nuclear accumulation upon transient (0.4M NaCl for 3 min, green) and sustained (from 0.075 to 0.4M NaCl in 20 min, red) activation of the pathway. Stepwise activation (dashed lines) for 0.075M (red), 0.1M (blue), 0.2M (cyan) and 0.4M NaCl (green) are shown for comparison. (**E**) Average signalling (red) and expression outputs (blue) for different activation patterns. The open and closed circles represent, respectively, the population of

non-reacting and reacting cells. Circle size is proportional to the population under each distribution. The error bars show the standard deviation of 40 to 130 single cells.

Figure 1

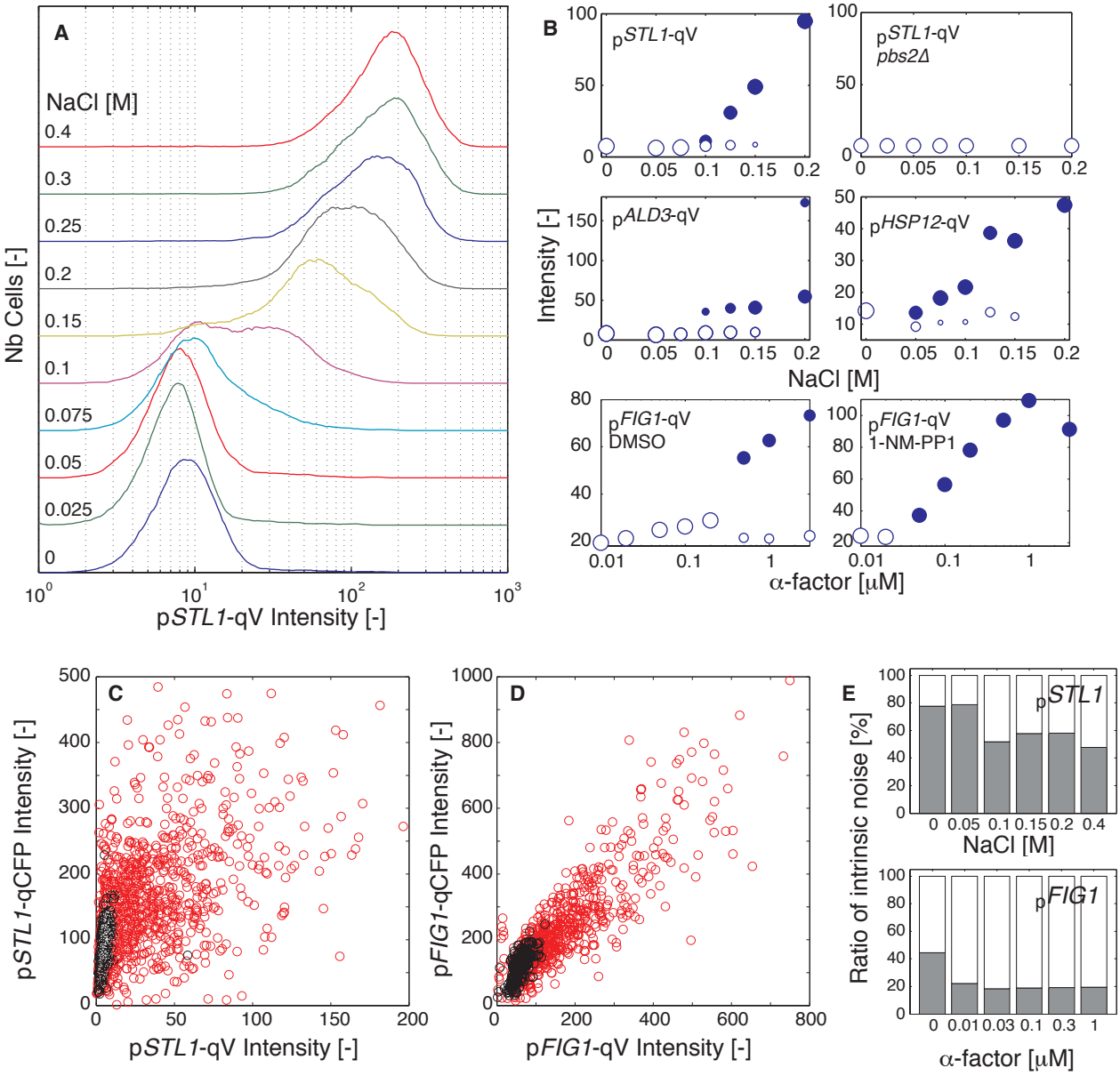
A
NaCl [M]
0.4
0.3
0.25
0.2
0.15
0.1
0.075
0.05
0.025
0
Nb Cells [-]
pSTL1-qV Intensity [-]
B
pSTL1-qV
pSTL1-qV
pbs2Δ
pALD3-qV
pHSP12-qV
pFIG1-qV
DMSO
pFIG1-qV
1-NM-PP1
Intensity [-]
NaCl [M]
α-factor [μM]
C
pSTL1-qCFP Intensity [-]
pSTL1-qV Intensity [-]
D
pFIG1-qCFP Intensity [-]
pFIG1-qV Intensity [-]
E
pSTL1
pFIG1
Ratio of intrinsic noise [%]
NaCl [M]
α-factor [μM]

Figure 2

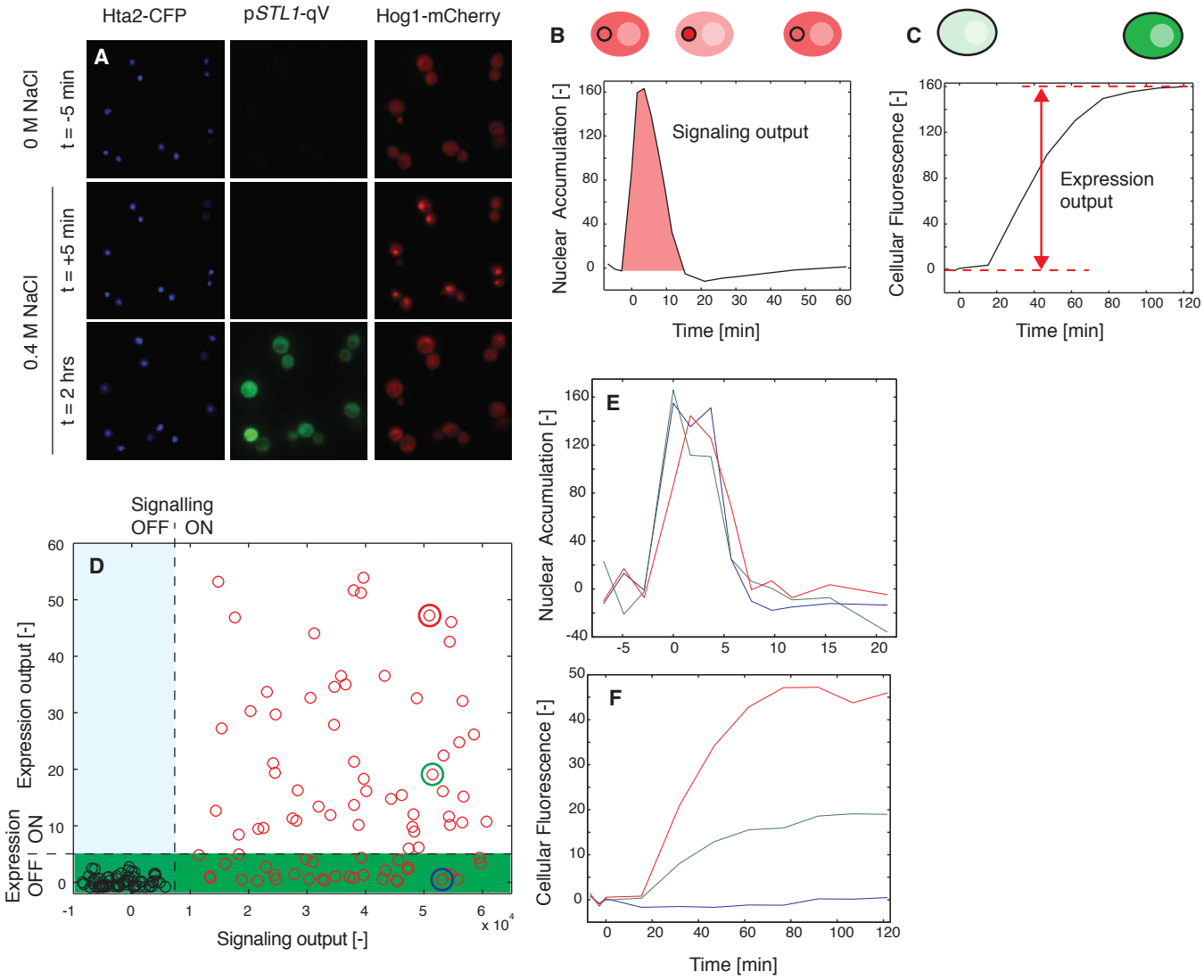
Hta2-CFP
pSTL1-qV
Hog1-mCherry
A
0 M NaCl
t = -5 min
0.4 M NaCl
t = +5 min
t = 2 hrs
B
Nuclear Accumulation [-]
Signaling output
Time [min]
C
Cellular Fluorescence [-]
Expression output
Time [min]
D
Signalling
OFF ON
Expression output [-]
Expression OFF ON
Signaling output [-]
x 10^4
E
Nuclear Accumulation [-]
F
Cellular Fluorescence [-]
Time [min]

Figure 3

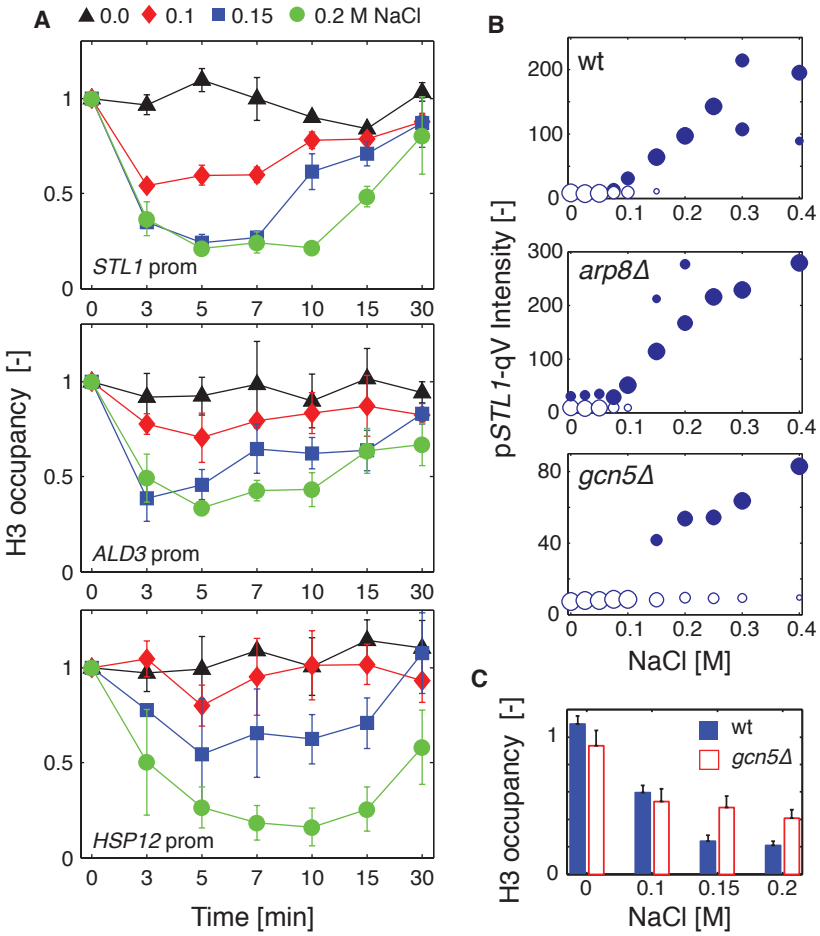
A
0.0
0.1
0.15
0.2 M NaCl
STL1 prom
ALD3 prom
HSP12 prom
H3 occupancy [-]
Time [min]
B
wt
arp8Δ
gcn5Δ
pSTL1-qV Intensity [-]
NaCl [M]
C
wt
gcn5Δ
H3 occupancy [-]
NaCl [M]

Figure 4

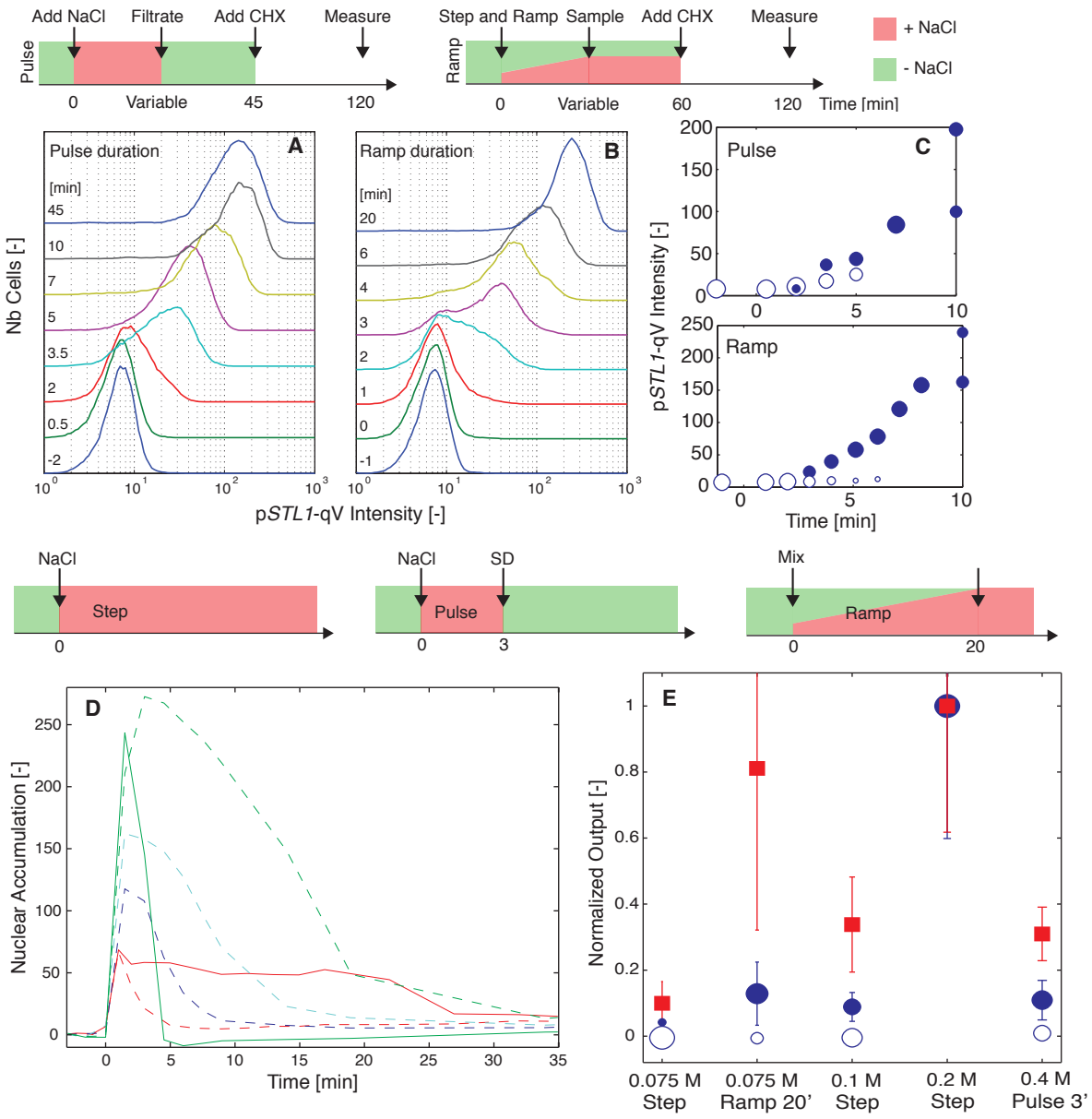
Add NaCl
Filtrate
Add CHX
Measure
Pulse
0
Variable
45
120
Step and Ramp
Sample
Add CHX
Measure
Ramp
0
Variable
60
120
Time [min]
+ NaCl
- NaCl
Pulse duration
[min]
45
10
7
5
3.5
2
0.5
-2
A
Ramp duration
[min]
20
6
4
3
2
1
0
-1
B
Nb Cells [-]
pSTL1-qV Intensity [-]
Pulse
C
Ramp
pSTL1-qV Intensity [-]
Time [min]
NaCl
Step
0
NaCl
SD
Pulse
0
3
Mix
Ramp
0
20
D
Nuclear Accumulation [-]
Time [min]
E
Normalized Output [-]
0.075 M Step
0.075 M Ramp 20'
0.1 M Step
0.2 M Step
0.4 M Pulse 3'

Supplementary Information

Transient activation of the HOG MAPK pathway regulates bimodal gene expression

Serge Pelet, Fabian Rudolf, Mariona Nadal-Ribelles, Eulàlia de Nadal, Francesc Posas and Matthias Peter

Methods

Yeast strains and Plasmids. Yeast strains and plasmids are listed in Tables S4 and S5. pRS-based reporter plasmids (*S1*) were constructed by cloning the different promoters amplified by PCR from yeast genomic DNA between SacI and XbaI, and the quadruple fluorescent protein cassette between HindIII and XhoI. The plasmids were integrated into wild-type yeast (W303 background) and stronger expressing transformants were selected by microscopy. Genes were deleted in the same reporter strains by mating or homologous recombination to avoid variations in expressions due to the integration of the fluorescent reporters.

Flow cytometry. Saturated overnight cultures grown in synthetic (SD) medium were diluted and grown for 24 hrs at log phase (below OD 0.4). The HOG pathway was induced by mixing 200µl culture with 100µl stress solution (SD medium + NaCl). Protein translation was stopped after 45 min by addition of cycloheximide (CHX, 0.1 mg/ml). Live cells were briefly sonicated, and fluorescence was measured by flow cytometry (FACSCalibur, BD, 488 nm excitation 530/30 nm emission) two to three hours after pathway induction. A similar protocol was used for other stresses: 200 µl of culture was induced by addition of 100µl stress solution (SD medium + diamide) to study oxidative stress, 200µl of culture were placed for 30 min, on a shaking heat-block at the desired temperature to observe the effect of heat stress. Translation was stopped with CHX 45

and 30 min, respectively, after induction. *Cdc28-as* cells were incubated for 15 min with at 15μM of inhibitor 1-NM-PP1 in DMSO or with DMSO alone (*S2*). 200μl of the inhibited and control cells were induced with 100μl of α-factor solution. After 45 min CHX was added to a final concentration of 0.1mg/ml.

Transient activation of the pathway was achieved by mixing 20 ml of culture with 10 ml of stress media. At the desired time points, 4 ml of the induced culture were filtered, the cells rinsed with 10 ml SD medium and then resuspended in 4 ml of SD. All samples were treated with CHX 45 min after the initial hyperosmotic shock and analyzed by FACS.

The ramping experiments were performed with 20 ml of culture to which 1 ml stress solution was added to reach a final concentration of 0.05 M NaCl. Then 4 M NaCl medium was slowly infused (0.092 ml/min) with a syringe pump (11 pico plus, Harvard Apparatus) for 20 min. 100μl aliquots were removed at various time points, treated with CHX one hour after stress induction and analyzed by FACS.

MATLAB (The MathWorks) was used to analyze the flow cytometry data. The measurements were gated using the forward and sideward scattering to retain mostly single cell data points. The calculated histogram was smoothed and fitted with one and two log-normal distributions. The best fit was selected by calculating the Akaike's information criterion (AICc) value and by visual inspection of the residuals. Due to the asymmetry in some FACS measurements, the double fit performs often better although the histogram does not represent a bimodal distribution. In these instances, the simpler single fit was selected.

Microscopy. Images were acquired on fully automated inverted epi-fluorescence microscopes (Axiovert 200M, Zeiss or Ti-Eclipse, Nikon) in an incubation chamber set at 30°C, with 60x or 40x oil objectives and appropriate excitation and emission filters. A motorized XY-stage allowed recording multiple fields of view at every time point. Well-

slides (LabTek 155411, Nunc) were coated with a filtered solution of Concanavalin A in PBS (0.5mg/ml) for 30 min and rinsed with H_2O. 200 µl of a diluted and briefly sonicated cell suspension (same growth conditions as described above) was added to the well. To quantify intrinsic and extrinsic noise cells bearing both fluorescent proteins were treated with NaCl or α-factor as described above for the FACS experiments. CHX was added 45 min after induction. The fluorescence was quantified by microscopy 2 to 3 hours after pathway induction.

For real-time measurements of the HOG pathway activation, 100 µl of a three fold concentrated solution of NaCl in SD medium was added to the well slide. Images were recorded at variable time intervals of 30 sec to 15 min. For pulsed activation of the pathway, microfluidic chambers (Y2 or Y4, Cellasic) were used to quickly change the medium surrounding the cells. Briefly, wells A were loaded with SD-full while wells B were loaded with SD-full + NaCl. The pressure was set to 5 psi resulting in an estimated flow rate of 10µl/hr. The flow surrounding the cells coming either from well A or B was switched by dedicated control software. Eight stage positions were imaged in chambers 1 and 2. The ramping experiments were performed in a flow chamber (µ-Slide IV, Ibidi) with cells attached to the bottom by Concanavalin A. Gravity flow (~3 ml/hr) was used to extract a small amount of medium from the mixing reservoir (20 ml) in which the concentration of NaCl was increased slowly using a syringe pump. Cells were imaged with an interval varying from 1 min at early time points to 15 min later on.

Image analysis. Images were automatically analyzed with MATLAB routines. For expression reporter measurements, cells were recognized using two bright field images at different focal planes. Edge detection was used to find groups of cells and a Hough transform allowed the identification of single cells. The average intensity from the segmented objects was calculated in the fluorescence images. For the Hog1 relocation experiments, individual cells were tracked using segmentation of the Hta2-CFP images to

identify their nuclei, while the cell area was obtained by segmentation of the RFP image. Based on the nucleus and cell objects, a third sub-nuclear region was defined with pixels contained in the cell object and within a distance of 5 pixels from the nucleus but not touching it. Hog1 nuclear accumulation was measured by calculating the difference in mean intensity between the nuclear and sub-nuclear objects in the RFP channel. This analysis removed artefacts due to bleaching and cell shrinking, which leads to a change in nuclear fluorescence intensity upon osmotic shock independent of Hog1 activation. The average intensity of the cell in the YFP channel was used to quantify the amount of fluorescent reporter expressed as function of time in each cell. Cells were assessed as expressing if their average fluorescence raised above the double of their initial auto-fluorescence intensity.

Chromatin-IP. Chromatin immunoprecipitation was performed as described previously (*S3*) using polyclonal anti-histone H3 antibodies (Abcam antibodies ab1791). Yeast cultures of wild-type (W303), and mutant strains (ySP167) were grown to early log phase before cells were exposed to different concentrations of NaCl for the indicated times. For cross-linking, yeast cells were treated with 1% formaldehyde for 20 min at room temperature. Quantitative PCR analysis was performed in real time using an Applied Biosystems 7700 sequence detector. Immunoprecipitation efficiencies were calculated in triplicate by dividing the amount of PCR product in the immunoprecipitated sample by the amount of PCR product in the input sample. The following primers with the indicated distance from the ATG initiation codon were used: *STL1* (-372/-112), *ALD3* (-180/+133), *HSP12* (-304/-82) and *TEL2* (region of 490 bp from right arm of chromosome VI) (SDS software Applied Biosystems). Data are presented as fold immunoprecipitation over *TEL2* sequence control. Images were quantified by Quantity One image software (BIORAD).

Supplementary Text

Model description:

We have established a simplified model of the HOG pathway to study the stochastic noise in gene expression (Table S2). To recapitulate the stochastic activation of the gene expression in single cells, we have used a stochastic solver (*S4, S5*). For these types of simulation the time constant of a reaction in s^{-1} indicates the propensity of a reaction to take place. The amount of each species in the model can only take integer value. At any time point, each reaction will have a given probability to occur based on the availability of the reactants and the time constant associated with this given step. Based on this probability, one reaction is randomly selected and performed transforming one unit of reactants into products as defined by the stoichiometry of the reaction. Due to the random selection of the reaction, the dynamics of the species will vary from one simulation to the next and therefore each simulation of the model will have a different outcome. Performing an ensemble simulation allows testing of a large set of possible outcomes for the model. This is therefore different than standard ODE models, in which rate constants define a fixed rate of reaction and each realisation of the model will lead to the same outcome.

The osmo-stress is represented by a STRESS agent, which can take values between 0 and 100. The adaptation of the cell is simulated by a first-order reaction, which slowly eliminates the stress agent. This simplified mechanism replaces the Hog1-dependent negative feedback loop that drives adaptation in living cells.

Since we have shown that signalling is not responsible for the apparition of bimodality in the expression (Fig. 2 and Fig. S3), we have minimized the number of up-stream components in the signalling cascade. The STRESS agent promotes therefore

directly the activation of the MAPK HOG1 (Hog1). Once active, HOG1-P can quickly be deactivated by a PHOSPHATASE (Ptp2 or Ptp3). These few reactions are sufficient to faithfully reproduce the general dynamics of the nuclear enrichment curves measured by microscopy in single cells.

In absence of stress, the TRANSCRIPTION FACTOR (TF, Hot1 or Sko1) is already bound to the GENE. After activation, HOG1-P is recruited to the gene via the TRANSCRIPTION FACTOR to stabilize the complex. This complex will in turn recruit POLII (polymerase) to form the INITIATION COMPLEX (*S6*). All these events are modelled with mass-action kinetics with the forward and backward reaction constants set to the same value. To achieve efficient transcription, remodelling of nucleosomes is necessary (*S7*). Therefore, we introduced an additional step in the model, which is the binding of the REMODELER (SAGA or RSC complexes) to form the ACTIVE GENE complex. We assumed that in cells once remodelled, the chromatin state stays open for a long period of time and therefore the back reaction was set a hundred time slower than the forward one.

Another mechanism was implemented to deactivate this complex through the action of the PHOSPHATASE, which can bind HOG1-P present in the complex. The PHOSPHATASE will thus inactivate HOG1-P and promote the disassembly of the whole complex. As long as HOG1-P is present, the PHOSPHATASE is mainly acting on the free MAPK pool since this rate constant was set three times higher than the one with HOG1-P involved in the transcription complex. Although this mechanism might seem artificial at first, it was implemented to reproduce the observation that mRNA production is limited to the time of Hog1 activity (*S8*). Moreover, this mechanism does not influence the ability of the model to generate a bimodal protein expression output.

Once assembled, the ACTIVE GENE complex can produce RNA, which in turn will be translated into PROTEIN. We implemented catalytic reactions for these two events such that a single reactant can produce multiple product molecules in consecutive reactions. We introduced a fairly rapid degradation of RNA, while we did not implement a degradation reaction for the protein, since the fluorescent proteins are known to have a long lifetime in the cells. The final protein production time course is similar to the apparition of fluorescence from the p*STL1*-qV reporter measured by microscopy, with the exception that the fluorescence apparition in the cell is delayed by 30 to 40 min due to the slow maturation of the chromophore.

The initial values for the various species of the model are given in the Table S3 (species not listed are set to zero). Since we wanted to focus on the expression of a single reporter gene, this number was naturally set to one. The number of Hog1 acting on that gene was extrapolated from the fact that roughly 200-400 genes are activated upon osmotic-stress (*S9*) and that there are roughly 7000 Hog1 molecules per cell (*S10*). Since only a fraction of active MAPK relocates to the nucleus, we made the conservative assumption that the number of active Hog1 per gene is on the order of 10. A larger number of HOG1 will only decrease the noise in the signalling cascade and not influence the noise in the expression output. The other species were all measured to be in the same order of magnitude as the number of Hog1-induced genes (*S10*) and were set to one. Anyway these values will only act as a scaling factor for the rate constant, since a single entity can bind to the active gene. As an example, if we set the number of TRANSCRIPTION FACTOR to 10, it will accelerate the binding reaction by an order of magnitude. However it will have no other influence on the simulation because once the GENE-TF complex is formed, the nine other TF present are not involved in any other reaction.

The rate constants given in Table S2 were used for all simulations presented in Fig. S8. Note that all time constants for this stochastic simulation have the units of s^{-1} since the species numbers are unit-less (*S4*). The values were chosen to reflect the known dynamics of various elements in the pathway such as Hog1 activation and protein expression measured in our experiments as well as mRNA production and ChIP time course data from Hog1, PolII and histone H3 on the *STL1* promoter (our data and (*S7*)). The major reactions that control the bimodal behaviour of the model are the three consecutive steps taking place on the GENE upon HOG1 phosphorylation to form the ACTIVE GENE complex. Since their rate constants are the same, we varied the forward and backwards reaction rates for the HOG1-P and POLII binding reactions together ($c_{hog\text{-}on}$ $c_{hog\text{-}on}$ $c_{pol\text{-}on}$ and $c_{pol\text{-}off}$) and in parallel varied the time constant of the remodelling reaction ($c_{rem\text{-}on}$). We show in Fig. S11 that a large range of values will generate a bimodal output for an initial number of STRESS agent of 3. The set of rate constants selected in the final model allowed a graded transition from a bimodal to a uniform expression as stress level is increased to mimic the measured flow cytometry data.

The SimBiology toolbox from MATLAB was used to design and simulate the model presented in Fig S8. Only uni-or bimolecular reactions with mass-action kinetics were implemented, since more complex kinetic implementations are not compatible with the stochastic simulation framework (*S11*). Using the stochastic solver, each run provides a possible outcome of the model due to the random occurrence of the individual reactions based on a Gillespie algorithm (*S4*). Ensemble simulation with 10'000 runs allowed exploring the space of the possible outcomes of the model. The final number of proteins obtained at the end of the run is converted to a simulated fluorescence level by the addition of a random number (normally distributed around 10 ± 5), which is small compared to the protein number (100 to 1000).

All simulations were started with 500 seconds (-500 to 0 s), where the number STRESS agent was set to 0. This allowed the various species to equilibrate in absence of STRESS. After this initial phase, the number of STRESS agents is set to a value between 0 and 100, which results in the activation of HOG1 and the execution of downstream reactions. For the pulse experiments, at a given time point after time zero, the STRESS is set back to 0, thereby shutting down the activation of HOG1 by the action of the PHOSPHATASE on free HOG1-P and HOG1-P in the ACTIVE GENE complex. For the sustained activation, the STRESS is set at 1 at time zero, but the adaptation time constant c_{adapt} is set to 0 for a given length of time, after which it is set back to its normal value of 0.003 s^{-1}, thereby recapitulating the absence of adaptation present during the ramp of NaCl concentration.

Although the model has some experimental prediction capabilities, it is evident that the dynamics of gene activation are not completely recapitulated by our simulations. In particular, the range of bimodal expression is typically larger in the model than in the measured data sets. The p*STL1*-qV expression is repressed at low stress levels and bimodality is only observed within a narrow concentration range until all cells express the fluorescent protein. This implies that the ultra-sensitivity of the mechanisms leading to the formation of activated target genes is stronger *in vivo* than in our simulations. We kept our model simple on purpose with only a few activation steps and used mass-action kinetics to demonstrate the basic mechanism needed for bimodal expression. However, in cells these processes are extremely complex with multiple transcription factors and chromatin remodelling complexes acting synergistically on the promoter. It is therefore not surprising that these highly cooperative processes generate a more switch-like response *in vivo*.

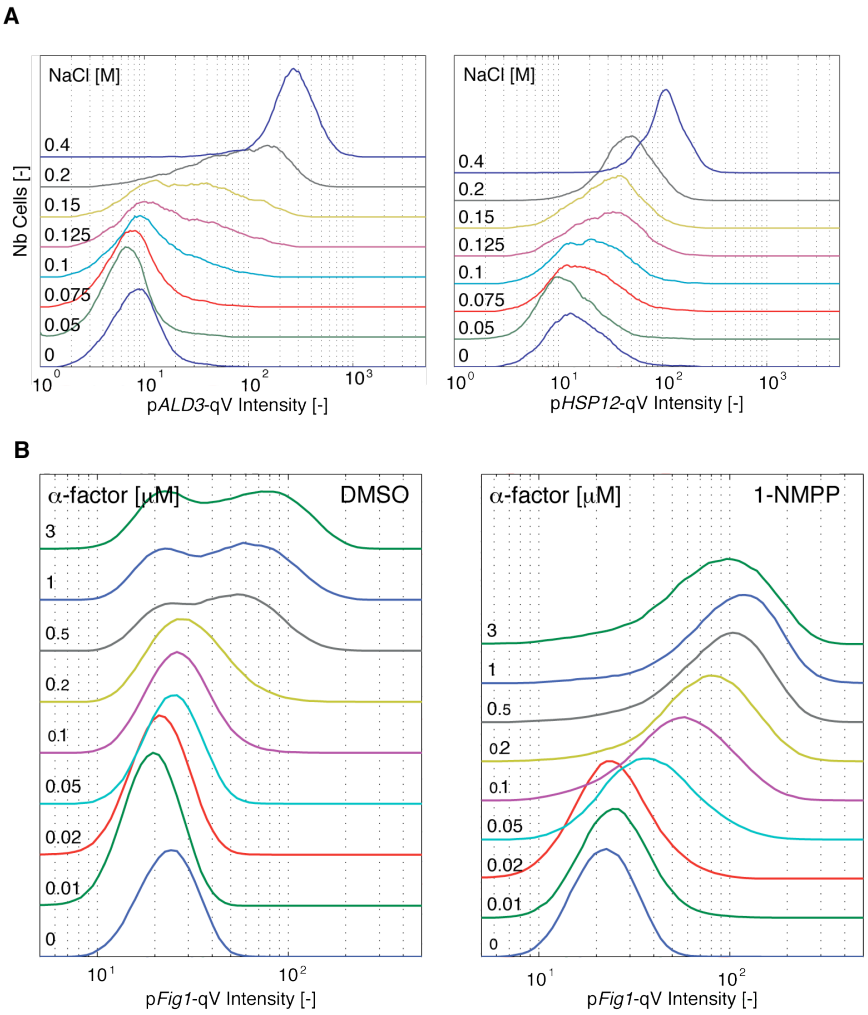

Fig. S1: Characterization of the expression reporters.

A. Flow cytometry histograms of dose response curves to NaCl of the quadruple Venus (qV) reporter driven by the stress-inducible promoters of *ALD3* (p*ALD3*-qV; left panel) and *HSP12* (p*HSP12*-qV; right panel). **B**. Flow cytometry profiles of dose response curves of the quadruple Venus (qV) reporter driven by the *FIG1*-promoter induced by α-factor for 45 min in a *cdc28-as* background treated with the analogue-sensitive kinase inhibitor 1-NM-PP1 (10μM) or its solvent DMSO for control. Addition of 1-NM-PP1 relieves the cell cycle regulation normally present in the mating signaling cascade and thereby allows all cells to signal uniformly.

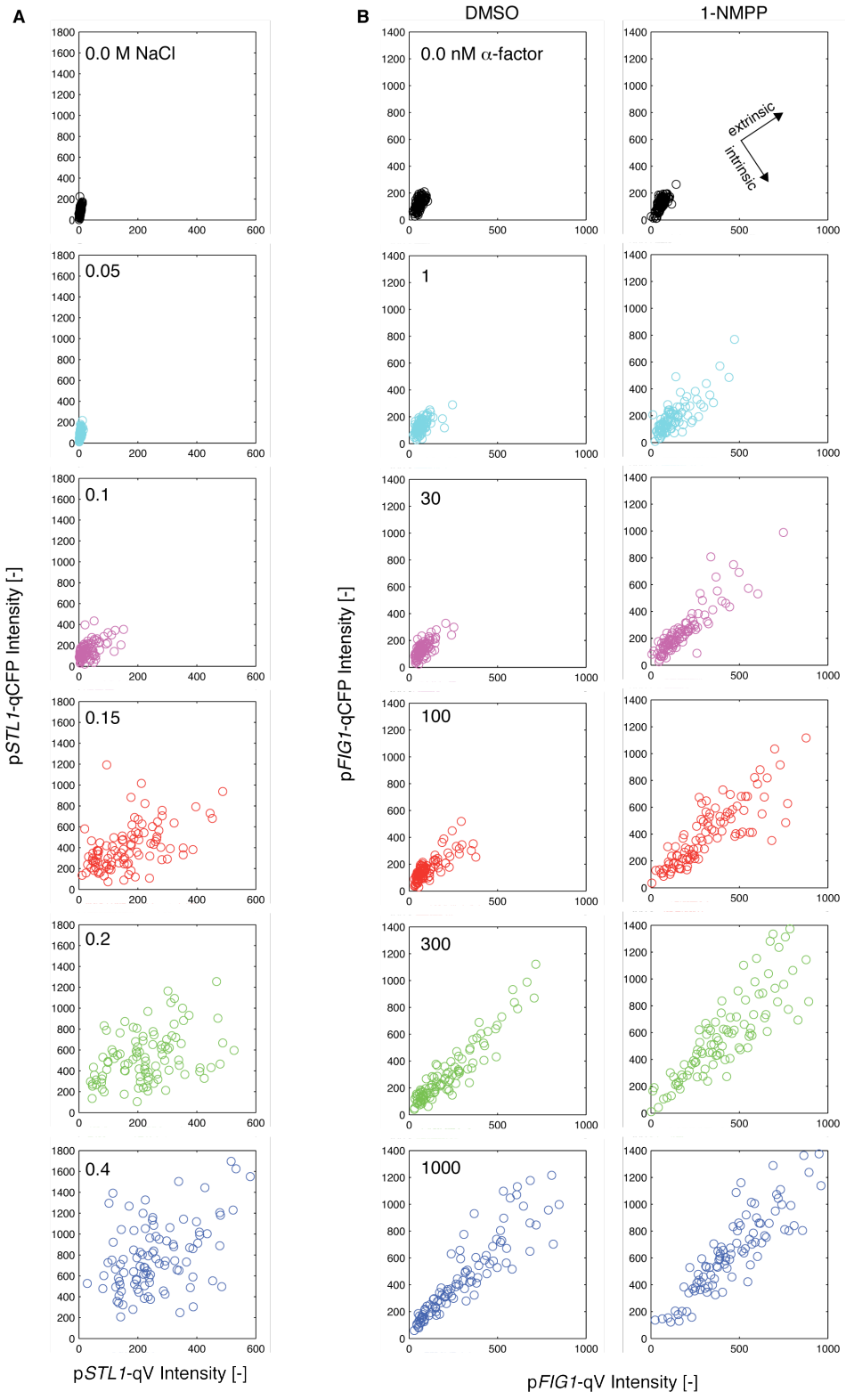

Fig. S2: Intrinsic and extrinsic noise in reporter induction.

A. Average cellular intensity in the YFP and CFP channels measured by microscopy in

cells containing the p*STL1*-qV and p*STL1*-qCFP reporters integrated at different loci. Reporter expression was induced by addition of the indicated NaCl concentrations. The strong intrinsic noise component is discernible by the lack of correlation between the CFP and YFP fluorescent intensities. **B.** Similar experiment as in panel A with cells containing the p*FIG1*-qV and p*FIG1*-qCFP expression reporters in the *cdc28-as* strain treated with DMSO or 10μM 1-NM-PP1. Expression was induced by addition of the indicated concentrations of α-factor. The significant correlation between CFP and YFP signals is indicative of important extrinsic noise regulation. A hundred cells are plotted in each graph out of the approximately 1000 cells measured to quantify the ratio of intrinsic and extrinsic noise.

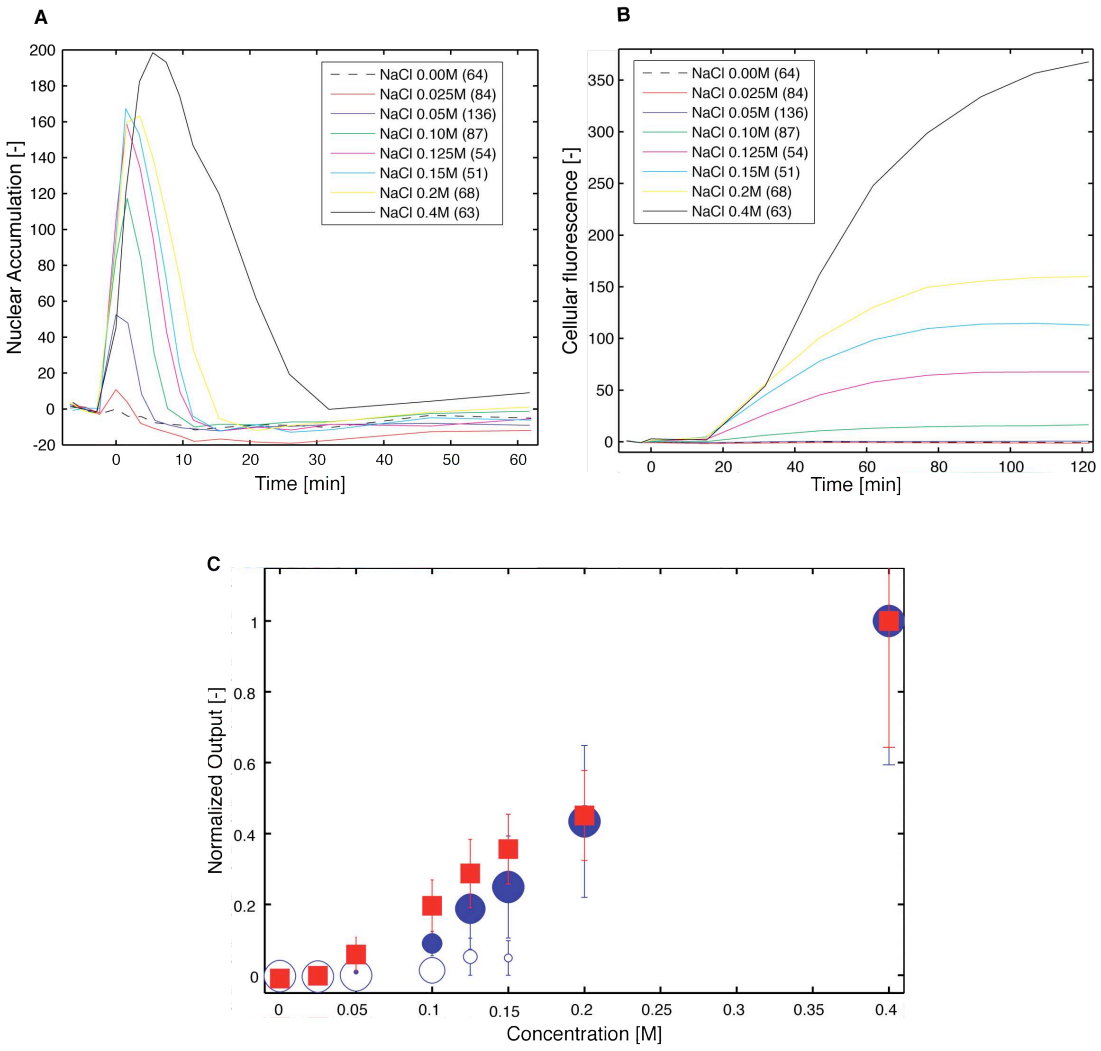

Fig. S3: Comparaison between HOG pathway activation and reporter expression.

A, B. Mean relocation of Hog1 (A) and reporter expression (B) calculated from single cell traces for the indicated NaCl concentrations. The number of cells averaged is listed in parenthesis. **C**. Mean expression- (circles) and signaling outputs (squares) from single cell traces as a function of NaCl concentration. The distribution of expression output measurements is split in expressing (filled markers) and non-expressing cells (open circles). The mean of each population is displayed in the graph and the size of the marker is proportional to the number of cells in each category. Error bars represent the standard deviation of 50 to 130 cells

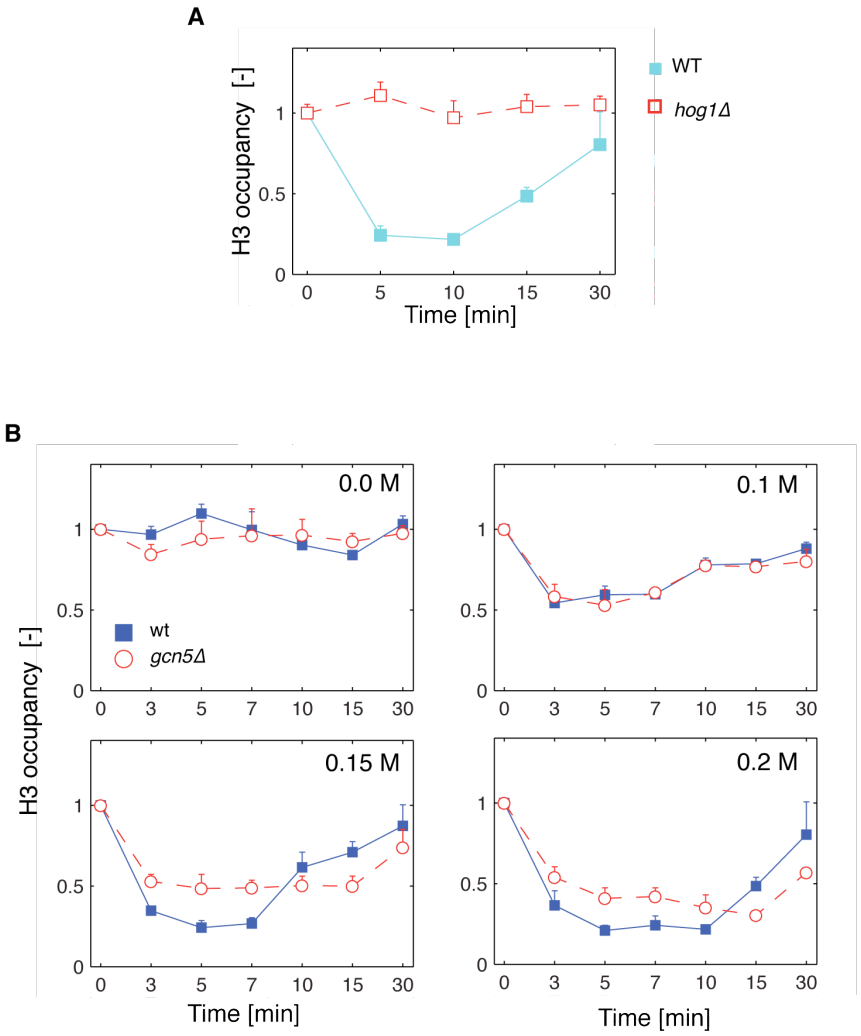

Fig. S4: Efficient eviction of histone H3 requires Hog1 and the SAGA complex.

A. H3 histone occupancy upon osmotic stress at the *STL1*-promoter in wild type (wt) and *hog1*Δ cells stressed with 0.2 M NaCl measured by quantitative ChIP experiments. Histone H3-binding was normalized to a *TEL2* sequence control. The error bars correspond to the standard deviation of three independent measurements. The eviction of the histone H3 is dependent on Hog1 activity. **B.** Dynamics of histone H3 eviction at the *STL1*-promoter in wild type and *gcn5*Δ cells at the indicated NaCl concentration. The lower eviction observed in the *gcn5*Δ cells correlates with the increased bimodal behavior measured by flow cytometry.

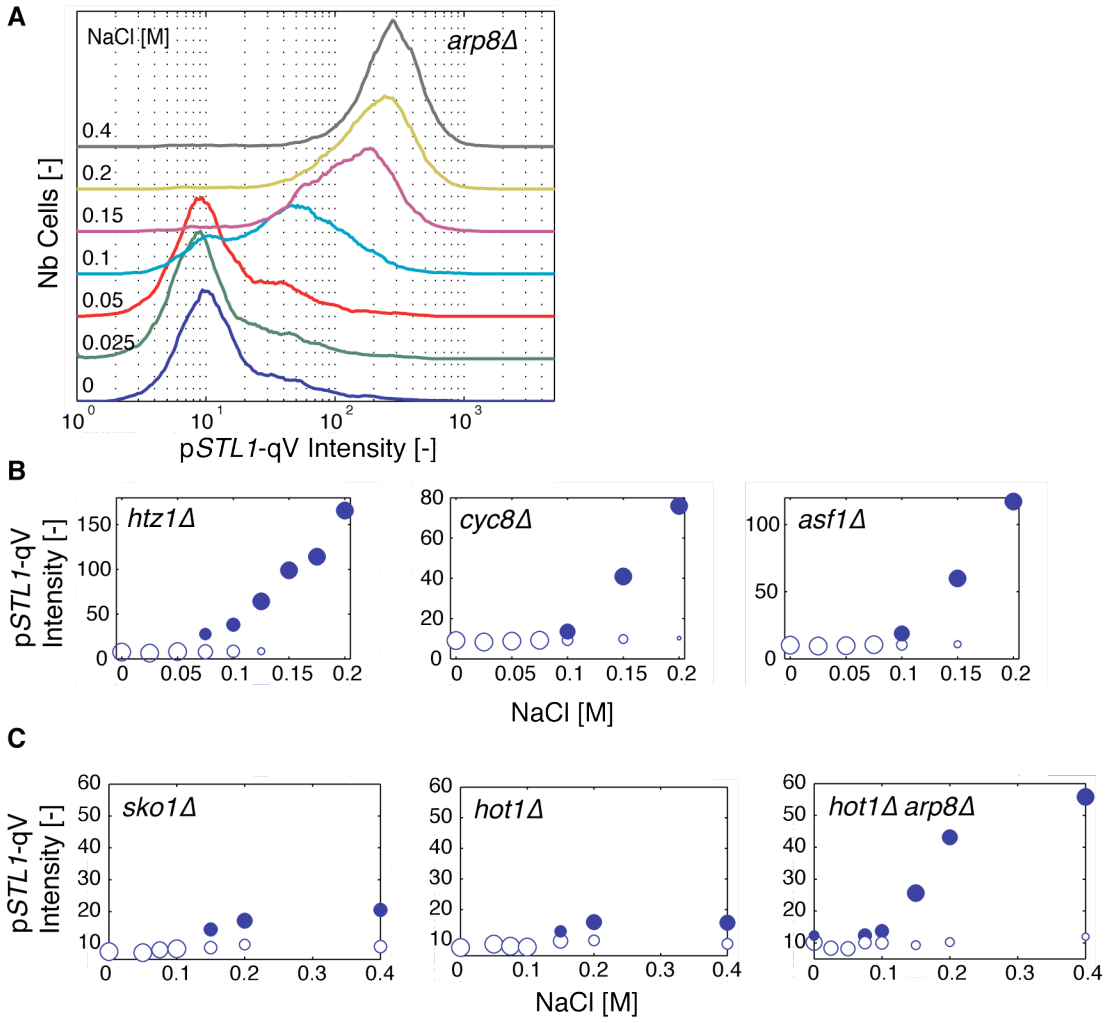

Fig. S5: Influence of various gene deletions on bimodal behavior

A. Flow cytometry histogram of the expression of the p*STL1*-qV reporter in *arp8*Δ cells. **B.** Log normal fits of flow cytometry histograms of p*STL1*-qV expression in *htz1*Δ, *cyc8*Δ and *asf1*Δ strains. The open and close circles represent the population of non-reacting and reacting cells, respectively. Other chromatin remodeling factors do not affect the bimodal expression behavior. **C.** Mean of the log-normal fit of flow cytometry histograms of p*STL1*-qVenus expression quantified in *sko1*Δ, *hot1*Δ and *hot1*Δ *arp8*Δ cells. Note that deletions of the transcription factors Hot1 and Sko1 influence the bimodality of gene expression, which is partly restored by simultaneous deletion of the INO80 subunit Arp8.

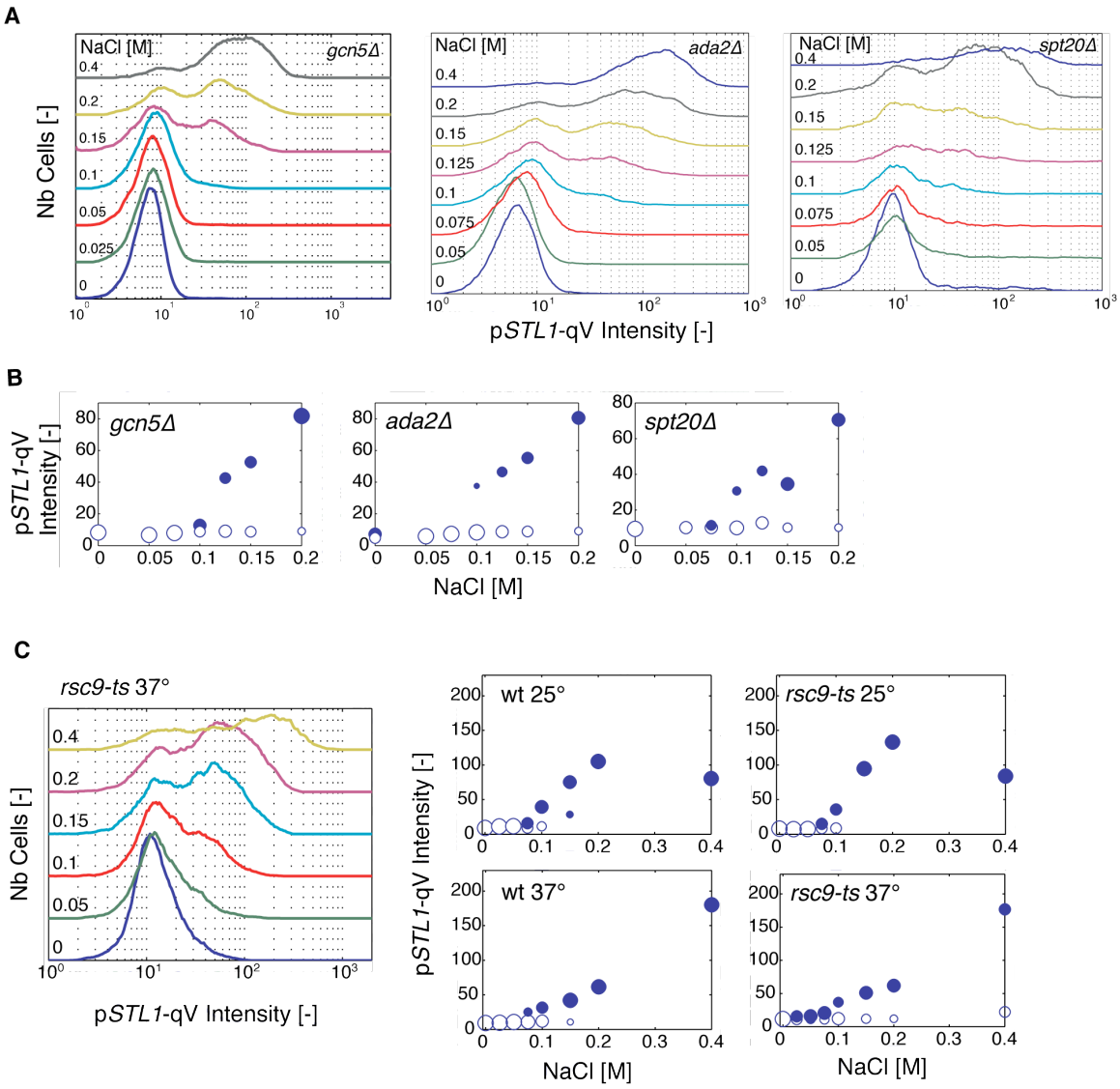

Fig. S6: The INO80, SAGA and RSC chromatin-remodeling complexes influence bimodal expression behavior.

A, B. Cells deleted for various components of the SAGA complex including *GCN5*, *ADA2* and *SPT20* display a comparable increase in bimodality of p*STL1*-qV expression. Histogram of flow cytometry measurements for *gcn5*Δ, *ada2*Δ and *spt20*Δ (A) and log-normal fits of the distributions (B) are shown. The open and close circles represent the population of non-reacting and reacting cells, respectively. **C.** *rsc9-ts* mutant cells defective at 37°C for nucleosome disassembly generate a phenotype similar to cells

lacking *GCN5*. Flow cytometry histogram and log-normal fits of wild type (wt) and *rsc9-ts* cells expressing the p*STL1*-qV reporter at permissive (25°) or shifted to restrictive (37°) temperature two hours before stress.

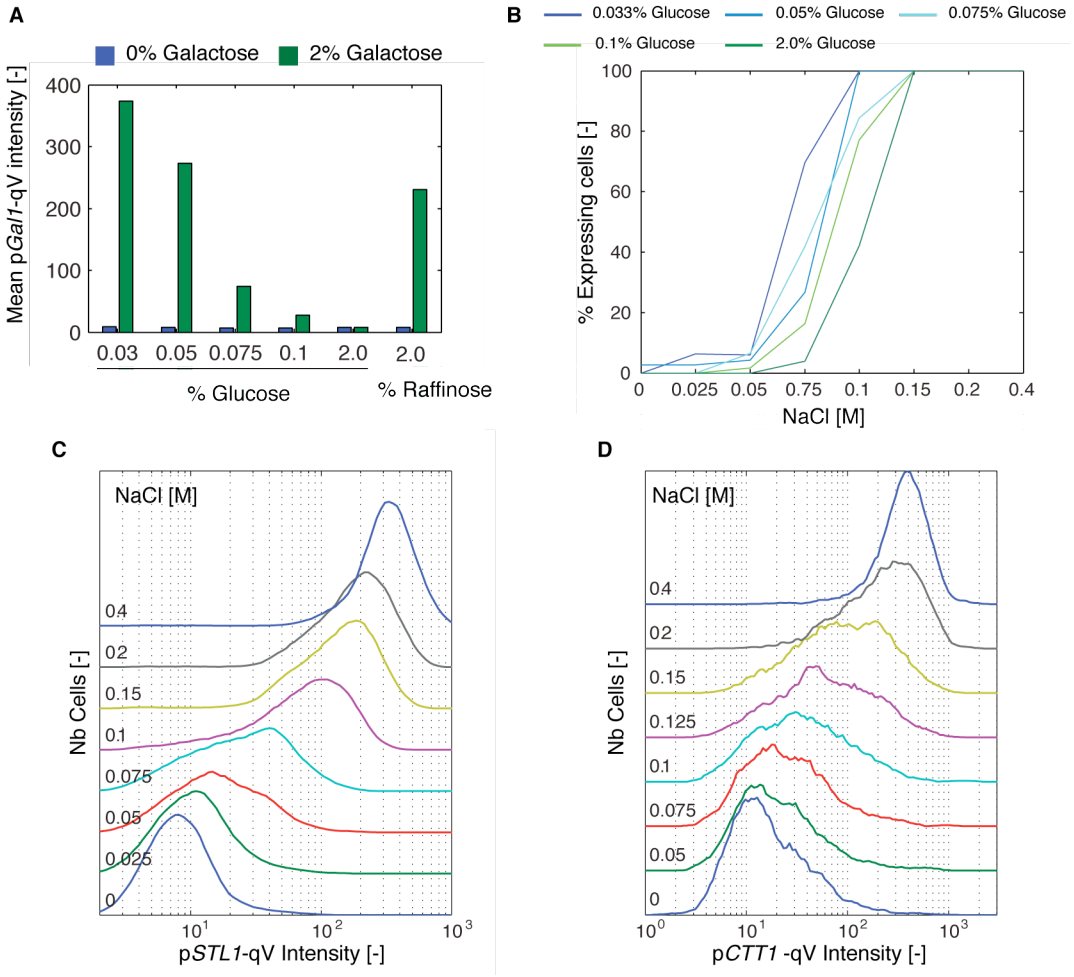

Fig. S7: Influence of glucose repression on bimodal expression of stress-induced genes

A. Induction of p*GAL1*-qV by 2% galactose for 45 min in cells grown in medium containing the indicated concentrations of glucose or raffinose. Complete de-repression of the *GAL1*-promoter occurs below 0.05% glucose. **B** and **C.** Cells bearing the p*STL1*-qV expression reporter were grown in various concentrations of glucose, stressed with NaCl as indicated, and the fluorescence was quantified by flow cytometry. Independently of glucose repression, these cells show a bimodal expression pattern. The concentration at which bimodality is observed increases with increased glucose repression (B). As an example the histogram of the dose response to NaCl for cells grown at 0.05% glucose is

shown in panel C. For low glucose experiments, the cells (p*GAL1*-qV or p*STL1*-qV) were grown overnight to saturation, filtered and resuspended in synthetic medium without glucose. The concentrated culture was diluted to OD 0.2 in medium with the desired glucose concentration. To keep the glucose concentration constant, cells were diluted two-fold every 90 min. After four hours of growth, the cells were challenged with galactose or NaCl. **D**. Bimodal expression is also observed with a p*CTT1*-qV expression reporter, which is not affected by glucose repression (*S12*). This demonstrates that glucose repression is not the sole mechanisms regulating bimodality.

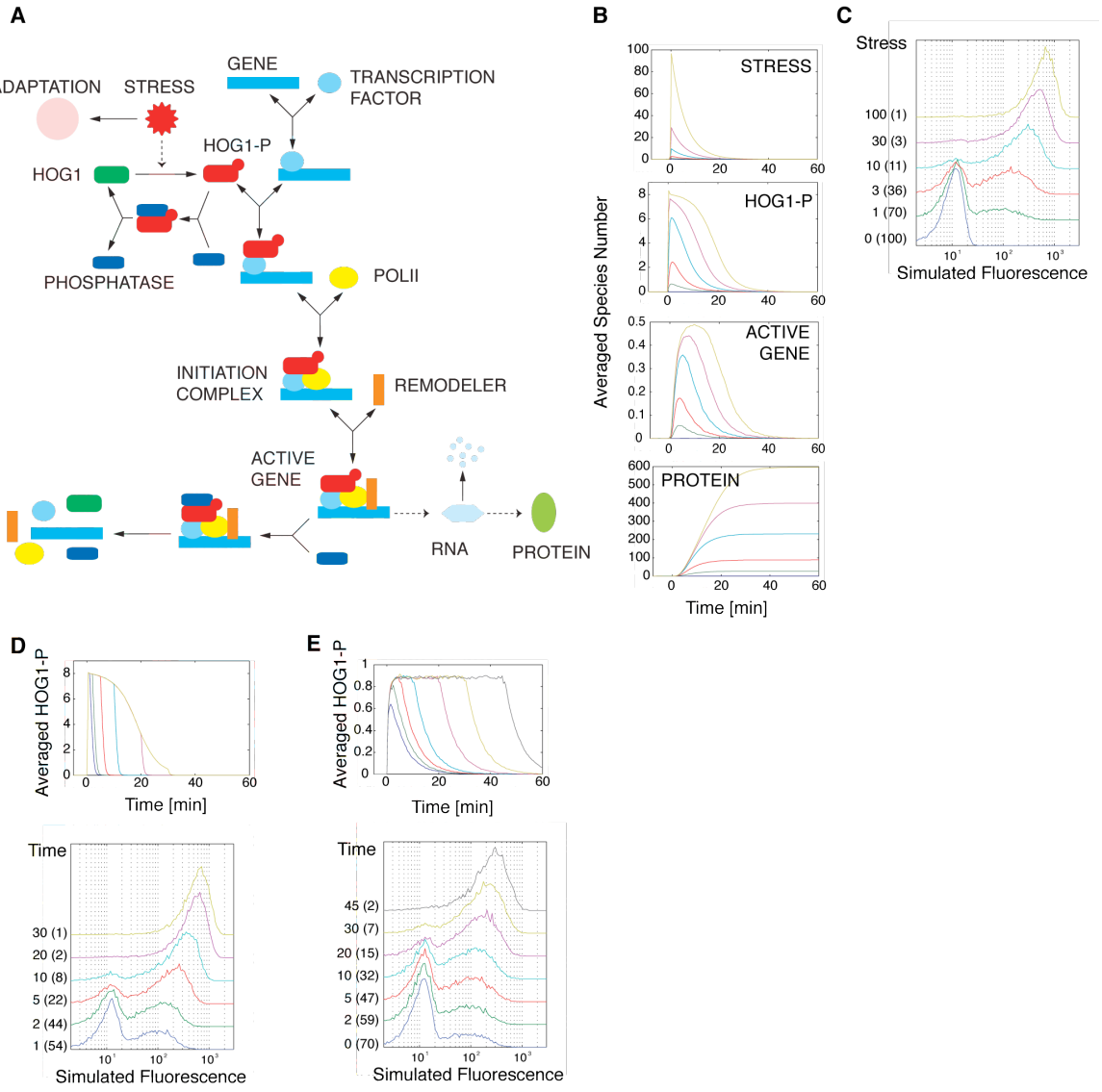

Fig. S8: Stochastic model of the transcription induction by Hog1.

A. Simplified scheme of the stochastic model. Dashed arrows represent catalytic reactions where the reactant is also a product of the reaction. **B.** Averaged species number upon stress activation plotted for STRESS agent, phosphorylated Hog1 (HOG1-P), ACTIVE GENE complex and PROTEIN as function of time for 10'000 stochastic simulations. The stress is set at different values between 0 and 100 at time 0. **C.** Histograms of the final simulated fluorescence for the different STRESS. The number in parenthesis indicates the percentage of runs resulting in absence of protein expression. **D**

and **E.** Averaged active Hog1 (HOG1-P) temporal evolution and the resulting simulated fluorescence histograms for transient activation of the pathway at high stress (D) or sustained activation of the pathway at low stress (E).

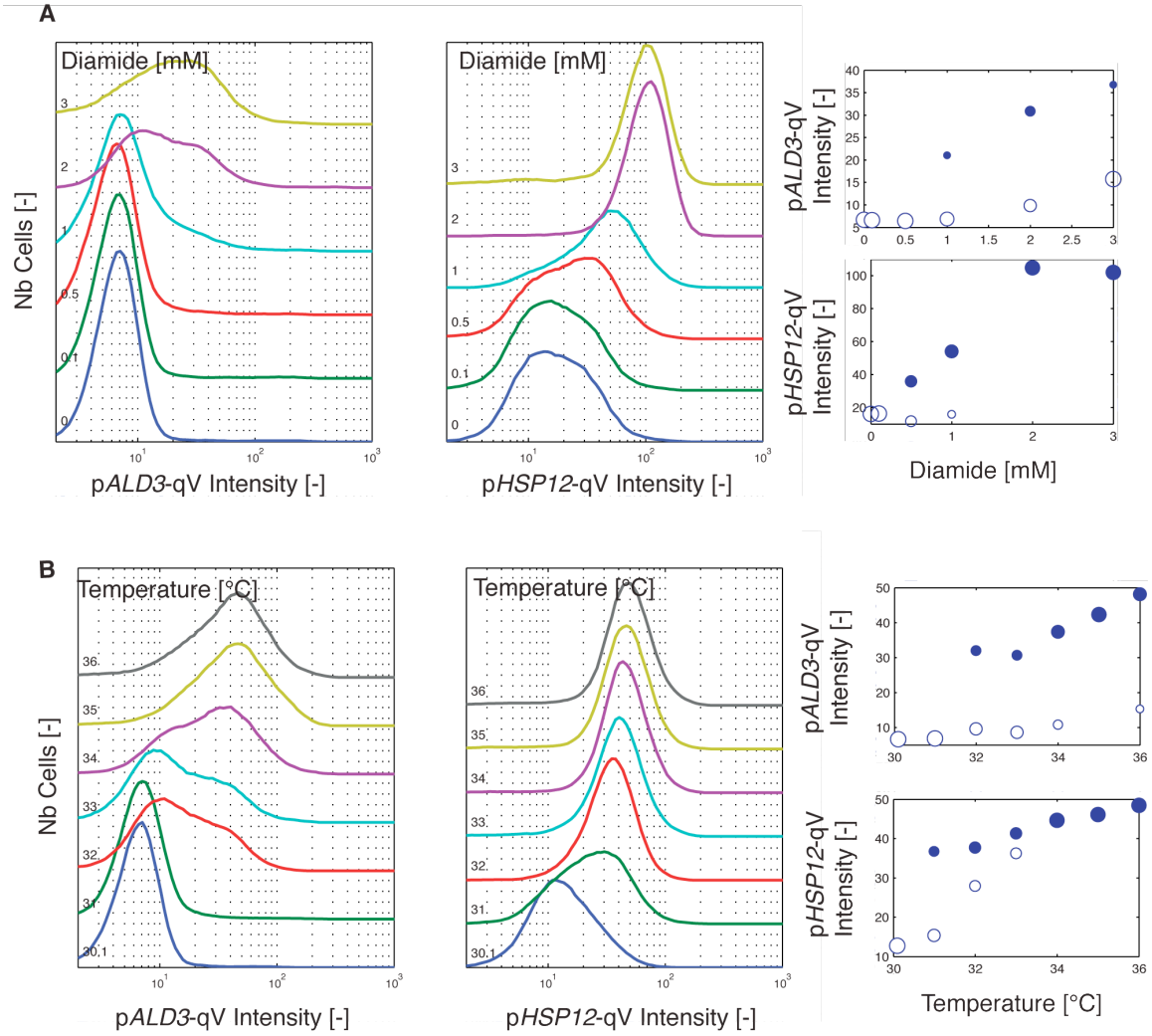

Fig. S9: Oxidative and heat stress generate bimodal gene expression

A. Flow cytometry histograms and mean of the log-normal fits of the fluorescent protein expression of p*ALD3*-qV and p*HSP12*-qV in response to oxidative stress induced for 45 min by various concentrations of diamide. **B.** Flow cytometry histograms and mean of the log-normal fits of the fluorescent protein expression of p*ALD3*-qV and p*HSP12*-qV in response to heat stress induced for 30 min by shifting cells grown at 30° to the indicated temperatures.

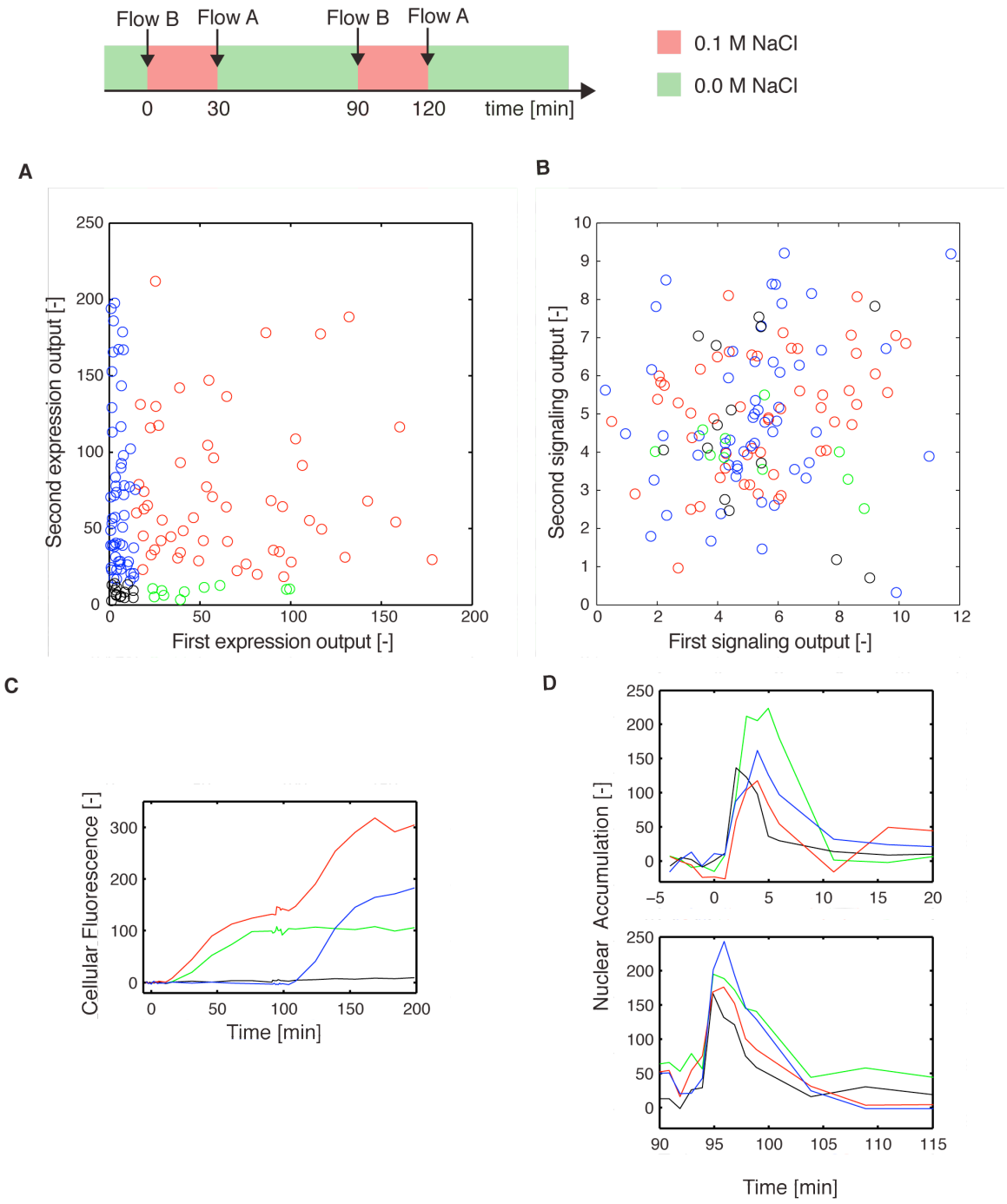

Fig. S10: Stochastic expression of fluorescent reporter upon double pulse of NaCl stress

A. Wild type cells expressing the nuclear marker Hta2-CFP, Hog1-mCherry and the p*STL1*-qV expression reporter were imaged in a microfluidic chamber. Cells were

exposed for 30 min to 0.1M NaCl osmotic stress and readapted to normal medium for 60 min. They were then subjected to a second 30 min pulse of 0.1M NaCl and shifted back to normal medium. The expression of the p*STL1*-qVenus reporter and nuclear accumulation of Hog1-mCherry were quantified for each stress pulse. The expression outputs in individual cells induced by the first pulse versus the second pulse are plotted. Black dots indicate cells that did not express. Green and blue dots represent cells expressing only after the first and second pulse, respectively, and red dots represent cells expressing after both osmotic stresses. **B.** The signaling outputs quantified for the first and second pulse for the same cells don't show any defined pattern. **C** and **D.** Single cell traces of the average cellular fluorescence in the YFP channel (C) and Hog1 nuclear accumulation in the RFP channel (D) for a cell that did not express (black) or expressed only after the first (green) or second (blue) pulse or expressed after both pulses (red).

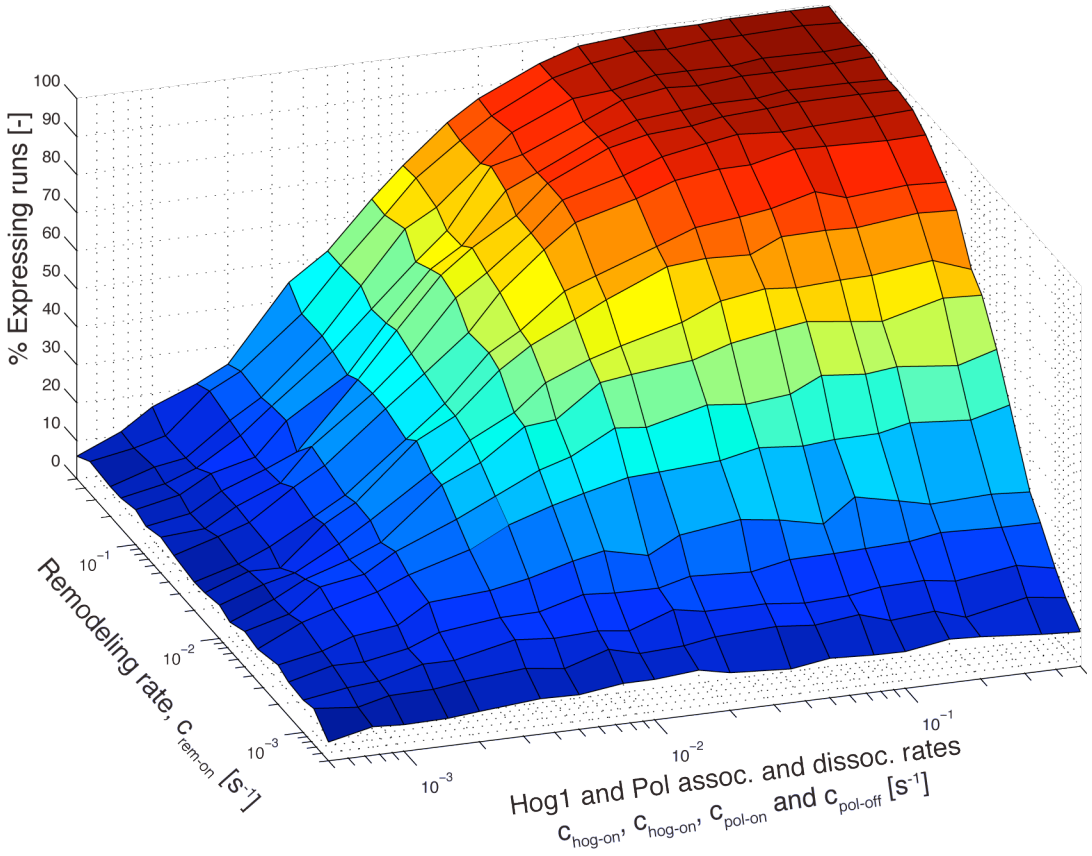

Fig. S11: Effect of stochastic rate constants on the bimodal output of the model. Variability in the bimodal behavior of the model as a function of chromatin remodeling and the stochastic rate constants of the Hog1 and PolII binding reactions for a stress agent number of 3.

Table S1: Expression level and threshold for expression of p*STL1*-quadruleVenus reporters in various strains.

Strain	Uninduced[a)]	Induced (0.4M NaCl)[a)]	Threshold[b)]
wt	3.0	100	0.1 (65%)
*pbs2*Δ	2.6	3.49	-
*ssk1*Δ	3.5	116	0.15 (64%)
*ste11*Δ	4.1	125	0.1 (54%)
*ptp2*Δ	2.9	74.6	0.1 (67%)
*nbp2*Δ	3.2	88	0.1 (64%)
*hot1*Δ	2.8	5.77	0.4 (50%)
*sko1*Δ	2.7	5.72	0.4 (52%)
*smp1*Δ	2.4	290	0.075 (58%)
*isw1*Δ	2.5	88.3	0.1 (72%)
*isw2*Δ	2.3	143	0.075 (35%)
*htz1*Δ	2.4	69.6	0.075 (39%)
*cyc8*Δ	5.9	89.2	0.1 (66%)
*set1*Δ	8.6	176	0.075 (22%)
*arp8*Δ	13.8	165	0.05 (30%)
*asf1*Δ	7.5	139	0.1 (69%)
*npl6*Δ	6.2	131	0.1 (64%)
*gcn5*Δ	4.2	49.7	0.15 (44%)
*spt20*Δ	8.9	65.2	0.125 (37%)
*ada1*Δ	6.4	72.3	0.15 (58%)
*ada2*Δ	3.5	74.8	0.125 (47%)
*rsc1*Δ	3.8	112	0.1 (34%)
*hat1*Δ	5.3	105	0.1 (62%)
*pdg1*Δ	5.8	104	0.1 (74%)
*hda1*Δ	7.0	109	0.1 (56%)
*snf6*Δ	5.5	152	0.1 (73%)
*rpd3*Δ	7.2	108	0.1 (51%)

[a)] Mean intensity measured by flow cytometry normalized to the intensity obtained in the wild type strain at 0.4 M NaCl.

[b)] NaCl concentration measured closest to fifty percent of expressing cells. In parenthesis is the percentage of expressing cells.

Table S2: Reactions and stochastic rate constants implemented in the model.

Reaction	Time constant	Value [s^{-1}]
Stress → ∅	c_{adapt}	0.003
Hog1 → Hog1-P	c_{basal}	1e-6
Hog1 + Stress → Hog1-P + Stress	c_{active}	0.005
Hog1-P +PTP → Hog1-P-PTP	$c_{ptp\text{-}on}$	0.1
Hpg1-P-PTP → Hog1 + PTP	c_{dephos}	0.1
Gene + TF → Gene-TF	$c_{tf\text{-}on}$	0.1
Gene-TF → Gene + TF	$c_{tf\text{-}off}$	0.1
Gene-TF + Hog1-P → Gene-TF-Hog1-P	$c_{hog\text{-}on}$	0.02
Gene-TF-Hog1-P → Gene-TF + Hog1-P	$c_{hog\text{-}off}$	0.02
Gene-TF-Hog1-P + PolII → InitComplex	$c_{pol\text{-}on}$	0.02
InitComplex → Gene-TF-Hog1-P + PolII	$c_{pol\text{-}off}$	0.02
InitComplex + Remodeler → ActiveGene	$c_{rem\text{-}on}$	0.01
ActiveGene → InitComplex + Remodeler	$c_{rem\text{-}off}$	0.0001
ActiveGene → ActiveGene + RNA	c_{rna}	0.05
RNA → ∅	$c_{rna\text{-}deg}$	0.01
RNA → RNA + Protein	c_{prot}	0.2
ActiveGene +PTP → ActiveGene-PTP	c_{deact}	0.03
ActiveGene-PTP → Gene + TF + Hog1 + PolII + Remodeler	c_{break}	0.1

Table S3: Initial amounts of species for stochastic simulation.

Species	Cellular concentration *in vivo*	Initial concentration *in silico*
Stress	-	0 - 100
Hog1	7000	10
Gene	200 - 400	1
Polymerase II	2000	1
Transcription Factor	150 - 500	1
Remodeler Complexes	1000 – 2000	1
Phosphatase	150 – 800	1

Table S4: List of yeast strains.

Strain	Genotype	Source /Ref
ySP2	Mata leu2-3,112 trp1-1 can1-100 ura3-1 ade2-1 his3-11,15	QUASI consortium
ySP9	Mata leu2::LEU2-p*STL1*-quadrupleVenus	this study
ySP33	Mata leu2::LEU2-p*ALD3*-quadrupleVenus	this study
ySP32	Mata leu2::LEU2-p*HSP12*-quadrupleVenus	this study
ySP301	Mata leu2::LEU2-p*FIG1*-quadrupleVenus his3::HIS3-p*FIG1*-quadrupleCFP	this study
ySP179	Mata leu2::LEU2-p*STL1*-quadrupleVenus his3::HIS3-p*STL1*-quadrupleCFP	this study
ySP143	Mata leu2::LEU2-p*STL1*-quadrupleVenus pbs2::Nat	this study
ySP111	Mata hta2::hta2-CFP leu2::LEU2-p*STL1*-quadrupleVenus hog1::hog1-mCherry-HIS3	this study
ySP164	Mata leu2::LEU2-p*STL1*-quadrupleVenus arp8::Nat	this study
ySP167	Mata leu2::LEU2-p*STL1*-quadrupleVenus gcn5::Nat	this study
ySP227	Mata leu2::LEU2-p*STL1*-quadrupleVenus ada2::Kan	this study
ySP225	Mata leu2::LEU2-p*STL1*-quadrupleVenus spt20::Kan	this study
ySP285	Mata leu2::LEU2-p*STL1*-quadrupleVenus rsc9::rsc9-ts-TRP	this study
ySP144	Mata leu2::LEU2-p*STL1*-quadrupleVenus hot1::Nat	this study
ySP250	Mata leu2::LEU2-p*STL1*-quadrupleVenus sko1::Kan	this study
ySP270	Mata leu2::LEU2-p*STL1*-quadrupleVenus arp8::Nat hot1::Kan	this study
ySP245	Mata leu2::LEU2-p*STL1*-quadrupleVenus htz1::Nat	this study
ySP162	Mata leu2::LEU2-p*STL1*-quadrupleVenus cyc8::Nat	this study
ySP165	Mata leu2::LEU2-pSTL1-quadrupleVenus asf1::Nat	this study
yAL56	Mata hog1::LEU2	this study
ySP222	Mata leu2::LEU2-p*CTT1*-quadrupleVenus	this study

Table S5: List of plasmids.

Plasmid	Insert	Backbone	Source /Ref
pSP34	p*STL1* (-800 -0) – quadruple Venus	pRS305	this study
pSP30	p*ALD3* (-664 -0) – quadruple Venus	pRS305	this study
pSP61	p*HSP12* (-800 -0) – quadruple Venus	pRS305	this study
pSP31	p*FIG1* (-450 -0) – quadruple Venus	pRS305	this study
pSP117	p*STL1* (-800 -0) – quadruple CFP	pRS303	this study
pSP170	p*FIG1* (-450 -0) – quadruple GFP	pRS303	this study
pSP62	p*CTT1* (-1000 -0) – quadruple Venus	pRS305	this study

Supplementary References

S1. R. S. Sikorski, P. Hieter, *Genetics* **122**, 19 (1989).
S2. A. C. Bishop *et al.*, *Nature* **407**, 395 (2000).
S3. M. Zapater, M. Sohrmann, M. Peter, F. Posas, E. de Nadal, *Molecular and Cellular Biology* **27**, 3900 (2007).
S4. D. T. Gillespie, *J Phys Chem-Us* **81**, 2340 (1977).
S5. D. T. Gillespie, *Annu Rev Phys Chem* **58**, 35 (2007).
S6. P. M. Alepuz, E. de Nadal, M. Zapater, G. Ammerer, F. Posas, *EMBO J* **22**, 2433 (2003).
S7. G. Mas *et al.*, *EMBO J* **28**, 326 (2009).
S8. E. de Nadal *et al.*, *Nature* **427**, 370 (2004).
S9. S. Hohmann, M. Krantz, B. Nordlander, *Meth Enzymol* **428**, 29 (2007).
S10. S. Ghaemmaghami *et al.*, *Nature* **425**, 737 (2003).
S11. D. T. Gillespie, *Physica A* **188**, 404 (1992).
S12. Z. Xu *et al.*, *Nature* **457**, 1033 (2009).